Journal of Photochemistry and Photobiology A: Chemistry 221 (2011) 84–89

Contents lists available at ScienceDirect

Journal of Photochemistry and Photobiology A: Chemistry

journal homepage: www.elsevier.com/locate/jphotochem

Functionalization of *rho*-ZMOF with photosensitizers for singlet oxygen generation

Simona Horsa, Kathryn Perez, Jaroslava Miksovska *

Department of Chemistry and Biochemistry, Florida International University, 11200 SW 8th Street, Miami, FL 33199, USA

ARTICLE INFO

Article history:
Received 6 December 2010
Received in revised form 10 April 2011
Accepted 24 April 2011
Available online 30 April 2011

Keywords:
Metal organic framework
Porous materials
Photosensitizers
Methylene blue
Phenosafranine

ABSTRACT

Here we report the functionalization of a zeolite-like-metal organic framework of RHO topology with two cationic photosensitizers, methylene blue (MB^+) and phenosafranine (PS^+). The spectroscopic properties of encapsulated MB^+ are strongly influenced by host–guest interactions. At low MB^+ loading levels, the photo-sensitizer remains monomeric and exhibits absorption and emission spectra that are red-shifted with respect to MB^+ spectra in aqueous solution. Strong interactions between MB^+ and the framework are clearly evident from the long fluorescence lifetime of the functionalized material, $\tau = 3.2$ ns, that is nearly an order of magnitude longer relative to MB^+ in aqueous solutions. Unlike MB^+, the larger diameter of PS^+ dye prevents its incorporation within the ZMOF framework and PS^+ molecules weakly bind to the external surface of the framework and exhibit absorption and emission properties similar to those measured for PS^+ in methanolic solution. The immobilized photosensitizers partially preserve their capacity to generate singlet oxygen as determined indirectly using diphenylanthracene as a chemical trap.

1. Introduction

Zeolite-like metal organic frameworks (ZMOFs) have attracted significant attention due to their elegant topology, relative ease of synthesis, and potential for applications in sensor technology, optoelectronics, separation, gas storage, and catalysis. This class of materials is based upon reticulating metal ions such as Zn, Cu, In, or Fe bridged by imidazole or imidazole derivatives and/or carboxylic acid groups associated with organic ligands [1]. The angle of the metal–imidazole–metal bond (145°) is comparable to the angle of the zeolitic Si–O–Si bond and allows for synthesis of three dimensional networks with topologies analogous to those found in zeolites. So far, 20 different mineral topologies have been identified in ZMOF frameworks, including zeolite-like topologies such as analcime (ANA), merlinoite (MER), zeolite Rho (RHO) and sodalite (SOD) [2]. The assignment of three letter symbols for metal organic frameworks was addressed by O'Keeffe et al. [3]. In one of the first synthesis of ZMOF materials Chen et al. obtained three Zn(II) 2-alkylimidazolates frameworks with ANA-, SOD-, and RHO zeolite topologies [4]. A non-solvothermal synthesis of extended ZMOFs of Zn(II)-imidazolate polymers with zeolitic topologies was reported by Tian et al. [5] employing solvents as structure directing agents. ZMOF with RHO and SOD topologies have been also prepared utilizing the bis-chelating bridging ligands: 4,5-dicarboxyimidazole, 4,6-pyrimidinecarboxylate, or 2-pyrimidinecarboxylate together with indium ions [6,7]. Yaghi's group have reported the synthesis of numerous zeolitic imidazolate frameworks based on Zn(II) or Co(II) metal centers connected by linkers of imidazole derivatives [1]. The authors showed that the combination of structure directing agents (amide solvent media) and organic linkers, together with strict reaction conditions are crucial for the synthesis of a wide variety of ZMOF structures [1]. Very recently, the synthesis of two metal organic polyhedra with SOD topology based on Pd(II) and tetrakis(1-imidazolyl)borate or hydrogen tetrakis(4-methyl-1-imidazolyl)borate was reported which display permanent porosity and stability in acidic and basic solution, was reported by the Yaghi's group [8], whereas the formation of boron imidazolate complexes with monovalent cations Li(I) and Cu(I) was described by Zhang et al. [9]. Synthesized ZMOF materials exhibit permanent porosity i.e., stability in the fully evacuated state, with relatively large cavity diameters ranging from ~3 Å to 27 Å, and high stability in water and alkaline solutions.

Unique ZMOF compositions and topologies containing well defined and structured internal cavities and channels, allow for further functionalization of the internal cavities. The physical properties of the internal surfaces can be fine-tuned either by covalent modification of the organic linkers or noncovalently through encapsulation of functional groups within the internal cavities. Since the synthesis of ZMOFs is highly sensitive to the reaction conditions, covalent modification of the organic linkers remains challenging [10]. To date, considerable effort has been focused on developing

Abbreviations: ANA, analcime net; MER, merlinoite net; MB^+, methylene blue; PS^+, phenosafranine; RHO, zeolite Rho net; SOD, sodalite net; AOT, sodium bis(2-ethylhexyl) sulfosuccinate; ZMOF, zeolite like metal organic framework.

* Corresponding author. Tel.: +1 305 3487406; fax: +1 305 3483772.
E-mail address: miksovsk@fiu.edu (J. Miksovska).

1010-6030/$ – see front matter © 2011 Elsevier B.V. All rights reserved.
doi:10.1016/j.jphotochem.2011.04.029

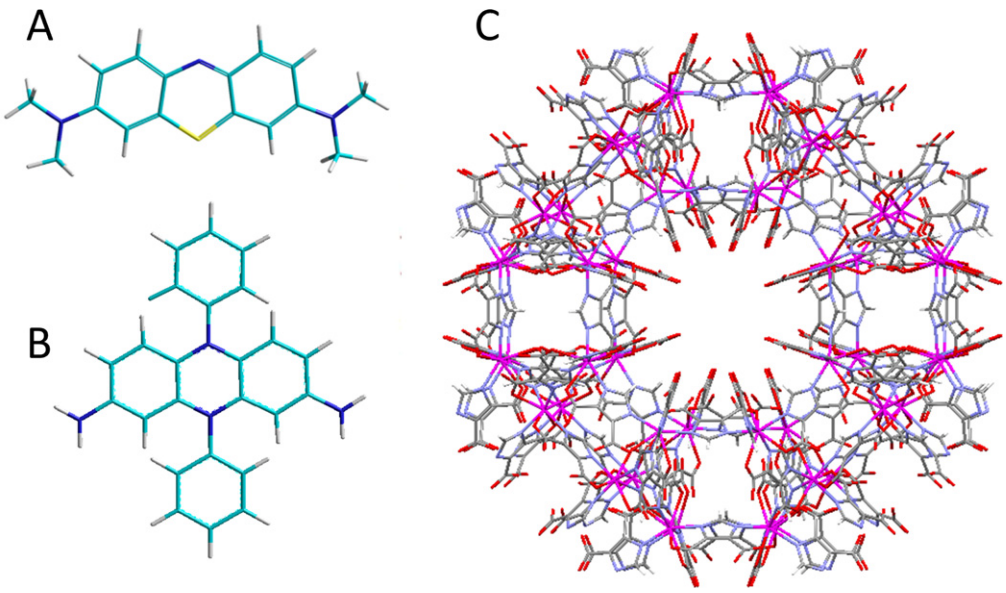

Fig. 1. Structure of MB^+ (A), PS^+ (B) and the rho-ZMOF α-supercage (C). For rho-ZMOF structure, carbon is shown in grey, indium in magenta, nitrogen in blue, oxygen in red, and hydrogen in white. (For interpretation of the references to color in this figure legend, the reader is referred to the web version of this article.)

highly porous ZMOF materials with a high capacity for gas storage as they have the potential to serve as low cost and lightweight sorbents with reversible and facile gas charge/discharge kinetics [11,12]. In contrast, ZMOF based heterogeneous catalysts offer several advantages relative to homogenous catalysts, including the ability to couple catalysis to chemical separation, encapsulation of molecular catalysts within the framework, substrate size selective catalysis, stabilization of reaction intermediates, catalysis utilizing the framework metal centers, and the development of multi-catalyst architectures. To date, only a few examples of the chemical catalysis by microporous metal organic frameworks have been reported. Among them, Cho et al. [13] has demonstrated a highly efficient porous framework based upon chiral (salen) Mn struts and Zn metal centers for enantioselective catalysts. In addition, Alaerts et al. have shown that benzene-1,3,5-tricarboxylate linkers can be explored as Lewis acid catalysts for the isomerization of α-pinene oxide, cyclization of citronellal and the rearrangement of α-bromoacetals [14]. Alkordi et al. [15] encapsulated Mn porphyrin within *rho*-ZMOF using the "ship-in-the-bottle" method and reported an enhanced catalytic activity for cyclohexane oxidation.

Here we report the functionalization of *rho*-ZMOF framework with two photosensitizers, methylene blue (MB^+) and phenosafranine (PS^+) and characterization of photophysical properties of this novel material. The structure of indium/4,5-dicarboxyimidazole based *rho*-ZMOF is composed of negatively charged cubooctahedral supercages (Fig. 1) connected through six octagonal prism linkers. The large diameter of supercages (18.2 Å) permits encapsulation of positively charged fluorescent probes or catalysts, whereas the restricted openings (6.8 Å in diameters) enable for free exchange of analytes or substrate/product molecules. Both MB^+ and PS^+ have been extensively employed as sensitizers in energy and electron transfer reactions due to their relatively high quantum yields for intersystem crossing (Φ_T) and $^1O_2$ generation ($\Phi_T = 0.5$ for MB^+ [16] and $\Phi_T = 0.2$ for PS^+ [17]) and long triplet state lifetime ($\tau_T = 79\ \mu s$ for MB^+ [18] and $\tau_T = 25\ \mu s$ for PS^+ [19]) as determined in the absence of oxygen. Our data shows that encapsulation of MB^+ within *rho*-ZMOF internal cavities influence the dye photo-physical properties due to the strong host–guest interaction, whereas the optical properties of PS^+ are only moderately altered by the framework. In addition, we have evaluated the possibility of using functionalized framework as photosensitizers.

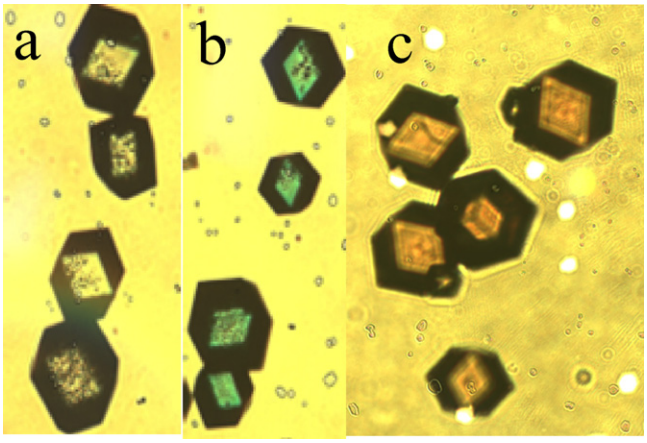

Fig. 2. Optical micrograph of *rho*-ZMOF crystalline material (a), MB-ZMOF (b), and PS-ZMOF (c).

2. Materials and methods

Methylene blue, phenosafranine, $In(NO_3)_2$, 4,5-dicarboxyimidazole and diphenylanthracene were purchased from Sigma–Aldrich and used as received. DMF and CH_3CN were obtained from Fisher-Scientific. *rho*-ZMOF crystals were synthesized according to the previously published procedure [6]. $In(NO_3)_3xH_2O$ (0.015 g) and 4,5-dicarboxy imidazole (0.014 g) were placed into a 20 mL glass vial and CH_3CN (1 mL), DMF (1 mL), 125 μL of HNO_3 in DMF (3.5 M in DMF) and 200 μL of 1,3,4,6,7,8-hexahydro-2H-pyrimido[1,2-a]pyrimidine (HPP) dissolved in DMF (0.42 M in DMF) were added. The vial was then sealed with a plastic cap and placed into a constant temperature oven (DKN 402, YAMATO). The temperature was then increased to 85 °C (2 °C/min heating rate) and heated at 85 °C for 12 h. Subsequently, the temperature was increased to 105 °C (1.5 °C/min heating rate) and held constant for 24 h. Finally the sample was cooled down to the room temperature with the rate of 1 °C/min. This approach provided ~20 mg of colorless hexagonal crystals as shown in Fig. 2. The crystals were then Na^+ exchanged by incubating them with aqueous solution of 2 M NaCl overnight and air dried. To

functionalize *rho*-ZMOF with MB^+, ~10 mg of *rho*-ZMOF material was dispersed in 2 mL of 5 μM aqueous solution of MB^+ and then intensively washed with ethanol and 2 M NaCl solution and dried on air. Relatively low concentration of MB^+ solution was for ZMOF functionalization with MB^+ to prevent formation of MB^+ dimmers within the framework. Exposure of ZMOF crystals to MB^+ solution of 10 μM or higher lead to dark blue crystals (data not shown). The *rho*-ZMOF framework was also incubated with 800 μM aqueous solution of PS^+ for 30 min. PS^+ functionalized crystals (PS-ZMOF) were then collected and washed with ethanol, and air dried prior to further analysis.

For UV–Vis and fluorescence measurements the functionalized crystals were attached to a glass slide by a thin layer of vacuum grease. The UV–Vis spectra were recorded using a single beam Carry 50 spectrophotometer. Fluorescence emission spectra and polarization were measured using PC-1 fluorimeter (ISS, Champaign, IL). The emission spectra and polarization data for MB^+ or PS^+ functionalized framework were detected using either 650 nm or 527 nm excitation wavelength. For polarization measurements the intensity of the emitted light was collected through either a 700 nm or 550 nm long pass filter (Andover Corp.), respectively. Polarization values were determined using, $p = (I_{II} - I_{\perp})/(I_{II} + I_{\perp})$ were I_{II} and $I_{\perp}$ are parallel and perpendicular intensities, respectively. The X-ray powder diffraction data were recorded using Siemens D500 X-ray diffractometer equipped with a Cu X-ray tube, a scintillation detector and an MDI databox. Data collection was performed using MDI Datascan software. The fluorescence lifetime measurements were performed on a home-built fluorescence lifetime instrument. The sample was excited with a 20 ps laser pulse (355 nm, 20 Hz, ~2 mJ/pulse, Continuum Leopard Nd:YAG laser) and the emission light was passed through a focusing lens, followed by a 400 nm long-pass optical filter (Andover Corp) and detected with a Si photodiode (EOT 2030, Electro-optics Inc., 300 ps rise/fall time). The signal was digitized using a 4 GHz digitizer (TDS7404, Tektronix). The traces represent the average of ~100 pulses. We were not able to determine the lifetime value for PS-ZMOF due to the small extinction coefficient of PS at 355 nm.

Singlet oxygen generation was monitored using diphenylanthracene (DPA) as a chemical trap. 10 mg of MB-ZMOF or PS-ZMOF crystals were placed into a 1 cm × 1 cm quartz cell and 2 mL of 40 μM DPA in methanol was added. The air-equilibrated solution was irradiated at 18 °C by a Xe lamp (250 W) using a 550 nm or 450 nm long pass filter to prevent direct excitation of DPA. The control experiments were conducted by illuminating *rho*-ZMOF crystals in the absence of a photo-sensitizer and by monitoring the changes in the DPA absorbance in the presence of MB-ZMOF or PS-ZMOF under dark conditions. Kinetic experiments were performed by monitoring the decrease of the absorbance bands of DPA as a function of irradiation.

3. Results and discussion

The high stability of rho-ZMOF framework in aqueous solutions and organic solvent allows for further framework functionalization using cation exchange approach. Exposure of *rho*-ZMOF crystals to 5 μM solution of MB^+ lead to a rapid uptake of MB^+ into the framework since a 30 min exposure provided light blue crystals, labeled MB-ZMOF, and colorless surrounding solution, indicating a strong affinity between the dye molecules and the *rho*-ZMOF framework. Subsequent intensive washing of the functionalized framework with ethanol (24 h) and 2 M NaCl (overnight) did not lead to the MB^+ release from the framework as shown in Fig. 4, inset. The fact that the exposure of MB-ZMOF to NaCl solution does not lead to dissociation of MB^+ from the framework points out that in addition to electrostatic interactions additional forces, such as van der Waals interactions between the dye and organic linkers stabilize MB^+ within internal cavities. On the other hand, exposure of *rho*-ZMOF crystals to 800 μM solution of PS^+ in methanol for 30 min and subsequent overnight washing with ethanol to remove nonspecifically bound PS^+ provided pink crystals labeled PS-ZMOF (Fig. 5). Subsequent washing with 2 M NaCl solution gave colorless crystals due to the dissociation of weakly bound PS^+ molecules (Fig. 5). These data are consistent with the fact that the smaller size of the MB^+ molecules (16 Å × 7 Å) permits the sensitizer to penetrate into the internal supercages and connecting channels whereas the larger dimensions of the PS^+ (11.5 Å × 9.6 Å) preclude diffusion into the framework, allowing only for weakly adsorption to the framework exterior surface, predominantly through electrostatic interactions between the dye molecules and the negatively charged framework.

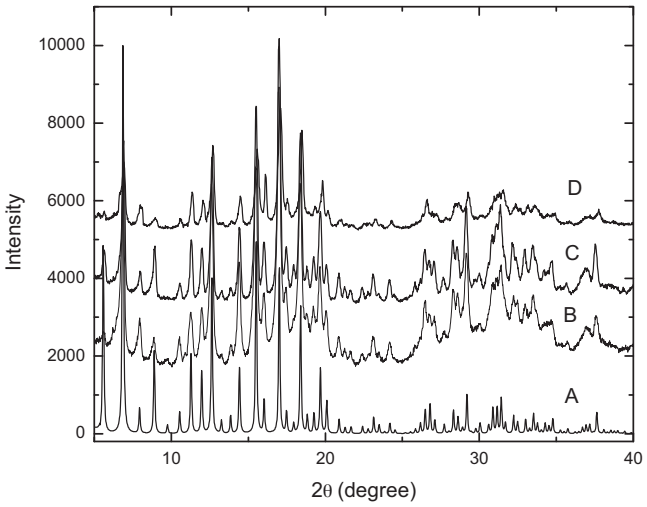

Fig. 3. Comparison of simulated X-ray powder diffraction pattern based on *rho*-ZMOF crystal structure (A) and experimental pattern for *rho*-ZMOF (B), MB-ZMOF (C), and PS-ZMOF (D).

The extent of dye loading/adsorption was determined by dissolving the crystals in 2 M aqueous solution of KCN and the concentration of the MB^+ and PS^+ was then measured spectroscopically using $\varepsilon_{664\,nm} = 8.5 \times 10^4\ M^{-1}cm^{-1}$ [20,21] and $\varepsilon_{520\,nm} = 5.4 \times 10^4\ M^{-1}cm^{-1}$ [19], respectively. For MB-ZMOF, the MB^+ loading was determined to be 1.5×10^{-4} μmol per mg of framework. The loading level for the MB^+ is lower than that for MB^+ loading in faujasite type zeolite Y which has been reported to be 2.5×10^{-3} μmol per mg of zeolite [22] and 5×10^{-4} μmol per mg of zeolite [23]. Indeed exposure of ZMOF framework to 1 mM MB^+ solution resulted in significantly higher value for MB^+ loading ~5.0×10^{-3} μmol per mg of framework that is comparable to values determined for zeolites. The concentration of PS^+ adsorbed on *rho*-ZMOF was measured to be 5.4×10^{-4} μmol per mg of *rho*-ZMOF. The integrity of the synthesized material was characterized using XPD crystallography. The XPD pattern of unmodified *rho*-ZMOF matches well the simulated XPD pattern (Fig. 3) as well as with the previously reported data [6], confirming the synthesis of the crystalline *rho*-ZMOF framework. More importantly, the same XPD pattern was recorded for *rho*-ZMOF functionalized with MB^+ or with PS^+ demonstrating that encapsulation of photosensitizer molecules within the framework internal cavities or its association on the surface do not perturb the structural properties of this material.

In order to investigate the photo-physical properties of MB^+ and PS^+ functionalized frameworks, the absorption and emission spectra were recorded. The absorption spectrum of MB-ZMOF, shown in Fig. 4, exhibits a maximum at 672 nm and an additional shoulder

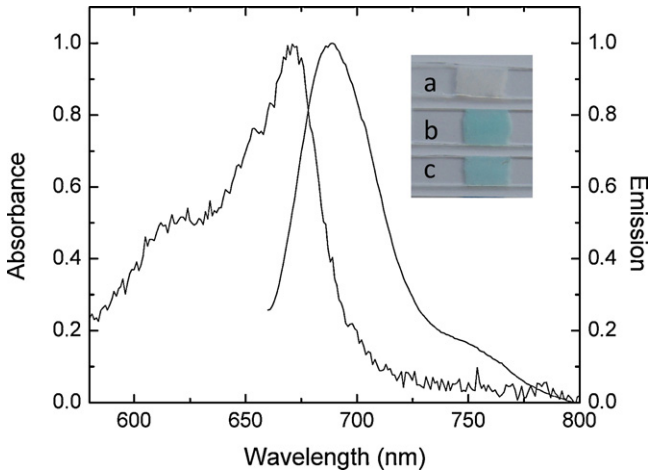

Fig. 4. Absorption and emission spectrum of MB-ZMOF (λ_{exc} = 650 nm) normalized to one. Inset: crystals of rho-ZMOF before functionalization (a), MB-ZMOF washed with ethanol (b) and subsequently with 2 M NaCl (c).

Table 1
Photo-physical properties of MB^+ and PS^+ in various environments.

	λ_{abs} (nm)	λ_{flu} (nm)	Polarization
MB-ZMOF	672 (620)	689 (746)	0.19
PS-ZMOF	527	570	0.28
MB^+ water	664 (610)	684	–
MB^+ methanol	653	680	0.07
PS^+ water	520	590	–
PS^+ methanol	527	570	0.04

Absorption and emission maxima ± 2 nm, the values in parenthesis correspond to the position of a shoulder band.

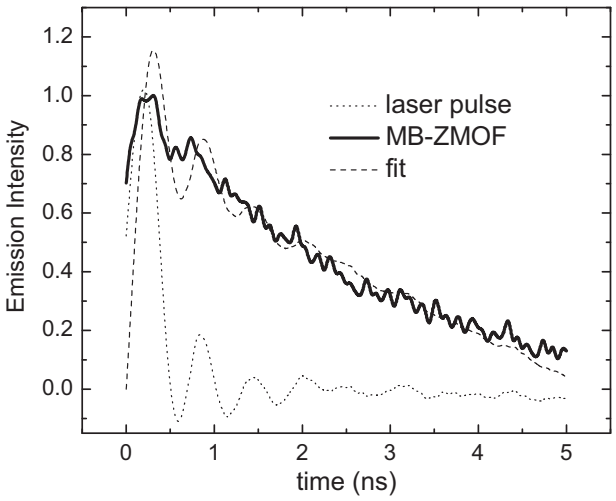

Fig. 5. Fluorescence lifetime trace of MB-ZMOF using λ_{exc} = 355 nm.

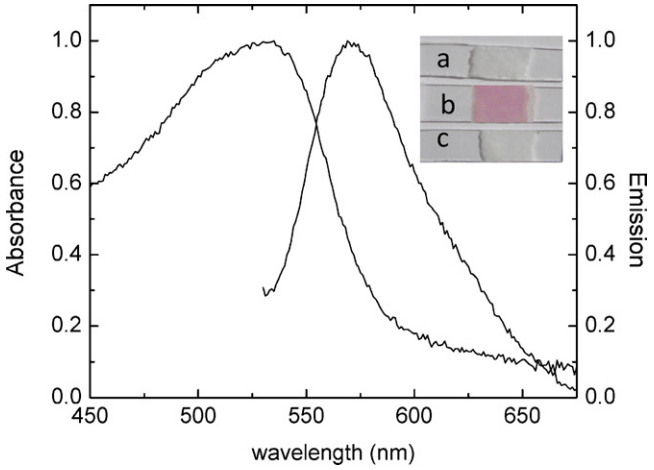

Fig. 6. Absorption and emission spectrum of PS-ZMOF (λ_{exc} = 500 nm) normalized to one. Inset: crystals of rho-ZMOF before functionalization (a), PS-ZMOF washed with ethanol (b) and PS-ZMOF washed with 2 M NaCl (c).

at 620 nm. This spectrum is consistent with the presence of predominantly monomeric dye within the framework. The spectrum is red-shifted relative to the spectrum of the MB^+ monomer in methanol and in water (Table 1) as well as in faujasite-type zeolite Y that was reported to have an absorption maximum at 665 nm and 667 nm [22,23]. We associate the observed bathochromic shift with the location of MB^+ near to highly polarizable, negatively charged sites within *rho*-ZMOF since comparable red-shift in the absorption spectrum was observed for acridine orange dye encapsulated within sodium bis(2-ethylhexyl) sulfosuccinate (AOT) reverse micelles [24]. The emission spectrum of MB-ZMOF is also red-shifted with respect to the monomer MB^+ spectra in water (λ_{flu} = 684 nm) and in methanol (λ_{flu} = 679 nm) and shows an emission maximum at 689 nm and additional shoulder located around 746 nm. The red-shifted emission spectrum further confirms strong interactions between the positively charged dye and negatively charged ZMOF. The unique character of the host–guest interactions are further confirmed by a relatively long fluorescence lifetime of MB^+ encapsulated within the ZMOF framework, τ = 3.2 ns, Fig. 5, which is roughly an order of magnitude longer than the lifetime of MB^+ in aqueous solution, τ = 380 ps [25]. We associated the increased fluorescence lifetime and the high polarization value determined for MB-ZMOF, p ~0.19 (Table 1) to the increase in structural rigidity and restricted molecular rotation of MB^+ encapsulated in *rho*-ZMOF.

The absorption spectrum of PS-ZMOF (λ_{max} = 527 nm), Fig. 6 shows significant broadening and has a similar maximum wavelength to that of PS^+ in methanol (Table 1) and close to spectra of PS^+ absorbed on NaY (λ_{max} = 522 nm) and ZMS-5 zeolites (λ_{max} = 520 nm) [26] indicating that adsorption of the sensitizer on the *rho*-ZMOF exterior surface does not significantly alter the ground state of PS^+ probe. The maximum of the fluorescence emission of the PS^+ functionalized framework is the same as the emission spectrum of PS^+ in methanol and slightly blue shifted with respect to the emission spectrum of PS^+ adsorbed on NaY and ZSM-5 zeolites [26]. Since the emission spectra are more sensitive to the polarity of the dye environment, these data suggest that the polarity of the external ZMOF surfaces is comparable to that of methanol whereas the red-shifted emission spectrum of MB-ZMOF indicates an increased polarity associated with the internal supercages. The relatively high polarization value observed here for PS-ZMOF (p = 0.28) corresponds to the restricted mobility of the dye adsorbed on the rho-ZMOF surface and/or may indicate a decrease in the singlet state lifetime due to the PS^+–framework interactions.

To explore the application of functionalized *rho*-ZMOF as a photosensitizer, the photochemical generation of singlet oxygen by MB-ZMOF and PS-ZMOF was probed by monitoring the photooxidation of diphenylanthracene (DPA) to its endoperoxide (Fig. 7, inset). Illumination of the functionalized MB *rho*-ZMOFs with visible light leads to the bleaching of the absorption bands of DPA, demonstrating the production of singlet oxygen (Fig. 7). A similar decrease in the absorption bands of DPA was observed in the case of PS-ZMOF illumination (data not shown). Illumination of the *rho*-ZMOF crystals in the absence of MB^+/PS^+ or incubation of MB-ZMOF/PS-ZMOF with DPA in the dark did not show any measurable decrease in DPA absorption at 371 nm, confirming

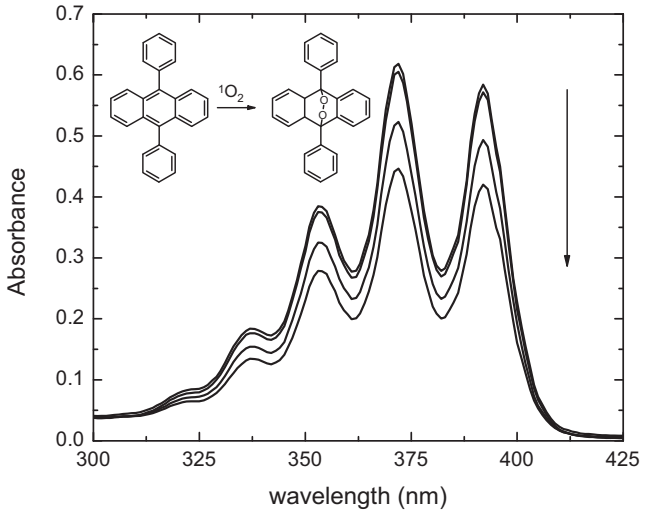

Fig. 7. Bleaching of the absorption bands of DPA when irradiated using MB-ZMOF as a photo-sensitizer. Inset: photo-oxidation of diphenylantracene (DPA).

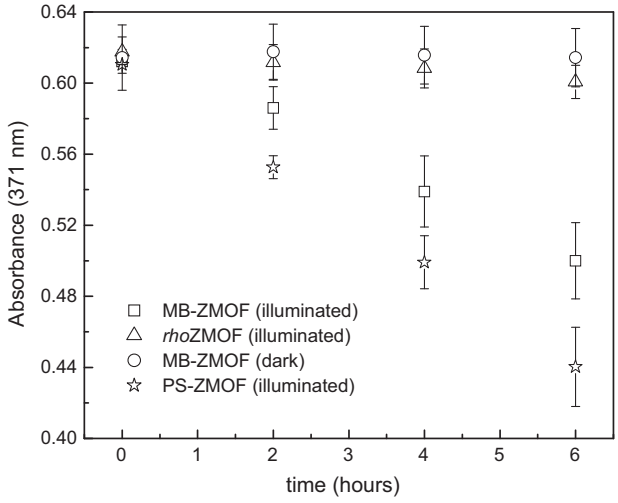

Fig. 8. Changes in the DPA absorbance at 371 nm in the presence of MB-ZMOF as a function of light exposure time. The data for the dark control and non-functionalized *rho*-ZMOF crystals are included. The data represent the average values from 3 independent measurements.

Table 2
Kinetic constants for DPA oxidation.

	Dye concentration (μM)	k_{obs} (10^{-2} h^{-1})
MB-ZMOF1	4.6	1.9 ± 0.1
MB^+ in solution	5.0	20 ± 1
PS-ZMOF	9.8	2.8 ± 0. 4
PS^+ in solution	13.0	5.1 ± 0.2

that the DPA bleaching is caused by $^1O_2$ production. The kinetic profiles for photosensitizer functionalized *rho*-ZMOF, either MB^+ or PS^+ were linear with time (Fig. 8). The observed kinetic constants for DPA oxidation were determined from the decrease of the absorption band of DPA at 371 nm as a function of time (Table 2) and were compared to the kinetic constants determined for MB^+ or PS^+ in the aqueous solution. The observed rate constant for the DPA oxidation by MB^+ in the solution is roughly ten times larger than that determined for MB-ZMOF using comparable concentrations of photosensitizer. The large diameter of the DPA molecule (~14.6 Å × ~9.2 Å) prevents incorporation of the singlet oxygen probe into the *rho*-ZMOF supercages. Thus, detection of $^1O_2$ molecules requires the reactive species to diffuse from the supercages into the bulk solution. Therefore, the smaller rate constant determined for DPA oxidation by MB-ZMOF relative to MB^+ in the solution is consistent with the relatively small fraction of $^1O_2$ molecules that can escape from the functionalized framework into surrounding solution within the singlet oxygen lifetime (~4 μs in water) [27]. Clearly, a considerable fraction of generated $^1O_2$ molecules is quenched either by residual water molecules situated within internal cavities or by dicarboxyimidazole linker in the *rho*-ZMOF framework. These data correspond to the results reported for the generation of singlet oxygen molecules within natural zeolites. Cojocaru et al. [28] have reported that a significant fraction of $^1O_2$ molecules generated within zeolites containing metal phthalocyanines or 2,4,6-triphenylpyryliyum photosensitizers escapes into the bulk media. On the other hand, the rate constant for DPA oxidation by PS-ZMOF is roughly 30% lower than that determined for PS^+ in solution under identical conditions implying that the PS^+ dye adsorbed onto the *rho*-ZMOF surface retain considerable efficiency for singlet oxygen generation.

4. Conclusion

The data presented here demonstrate unique guest–host interactions between a MB^+ photosensitizer and the internal cavities of the *rho*-ZMOF framework. The fact that the absorption and emission spectra of the PS^+ associated with the external framework surface are similar to those of PS^+ solubilized in methanol further illustrates the unique environment of the *rho*-ZMOF supercages. More importantly, the functionalization of *rho*-ZMOF with MB^+ or PS^+ photosensitizers demonstrates the potential for photoactive metal organic frameworks, to serve as photocatalysts.

Acknowledgments

Authors would like to acknowledge Dr. Randy Larsen, Department of Chemistry at University of South Florida for an assistance with time-resolved measurements, Dr. Kathleen Rein, Department of Chemistry and Biochemistry, Florida International University, for microscope measurements and Dr. James Talbot, KT GeoServices, Inc., Gunnison, CO for XPD measurements. The research was supported by J. & E. Biomedical Research Program (Florida Department of Health, J.M.) and National Science Foundation (MCB 1021831, J.M.).

References

[1] K.S. Park, Z. Ni, A.P. Côté, J.Y. Choi, R. Huang, F.J. Uribe-Romo, H.K. Chae, M. O'Keeffe, O.M. Yaghi, Exceptional chemical and thermal stability of zeolitic imidazolate frameworks, Proc. Natl. Acad. Sci. U.S.A. 103 (2006) 10186–10191.
[2] A. Phan, C.J. Doonan, F.J. Uribe-Romo, C.B. Knobler, M. O'Keeffe, O.M. Yaghi, Synthesis, structure, and carbon dioxide capture properties of zeolitic imidazolate frameworks, Acc. Chem. Res. 43 (2010) 58–67.
[3] M. O'Keeffe, M.A. Peskov, S.J. Ramsden, O.M. Yaghi, The reticular chemistry structure resource (RCSR) database of, and symbols for crystal nets, Acc. Chem. Res. 41 (2008) 1782–1789.
[4] X.-C. Huang, Y.-Y. Lin, J.P. Zhang, X.-M. Chen, Ligand-directed strategy for zeolite-type metal-organic frameworks: zinc(II) imidazolates with unusual zeolitic topologies, Angew. Chem. 45 (2006) 1557–1559.
[5] Y.-Q. Tian, Y.-M. Zhao, Z.-X. Chen, G.-N. Zhang, L.-H. Weng, D.-Y. Zhao, Design and generation of extended zeolitic metal-organic frameworks (ZMOFs): synthesis and crystal structure of zinc(II) imidazolate polymers with zeolitic frameworks, Chem. Eur. J. 13 (2007) 4146–4154.
[6] Y. Liu, V.C. Kravtsov, R. Larsen, M. Eddaoudi, Molecular building blocks approach to the assembly of zeolite-like metal-organic frameworks (ZMOFs) with extra-large cavities, Chem. Commun. 14 (2006) 1488–1490.
[7] D.F. Sava, V.C. Kravtsov, F. Nouar, L. Wojtas, J.F. Eubank, M. Eddaoudi, Quest for zeolite-like metal-organic frameworks: on pyrimidine carboxylate bis-chelating bridging ligands, J. Am. Chem. Soc. 130 (2008) 3768–3770.
[8] Z. Lu, C.B. Knobler, H. Furukawa, B. Wang, G. Liu, O.M. Yaghi, Synthesis and structure of chemically stable metal-organic polyhedra, J. Am. Chem. Soc. 131 (2009) 12532–12533.

[9] J. Zhang, T. Wu, C. Zhou, S. Chen, P. Feng, X. Bu, Zeolitic boron imidazolate frameworks, J. Am. Chem. Soc. 48 (2009) 2542–2545.
[10] R.A. Fischer, C. Woell, Functionalized coordination space in metal-organic framework, Angew. Chem. Int. Ed. 47 (2008) 8164–8168.
[11] N.L. Rosi, E. Juergen, M. Eddaoudi, D.T. Vodak, J. Kim, M. O'Keeffe, O.M. Yaghi, Hydrogen storage in microporous metal-organic frameworks, Science 300 (2003) 1127–1129.
[12] F. Nouar, E. Juergen, J.F. Eubank, P. Forster, M. Eddaoudi, Zeolite-like metal-organic frameworks (ZMOFs) as hydrogen storage platform: lithium and magnesium ion-exchange and H_2–(rho-ZMOF) interaction studies, J. Am. Chem. Soc. 131 (2009) 2864–2870.
[13] S.-H. Cho, B. Ma, S.B. Nguyen, J.T. Hupp, T.E. Albrecht-Schmitt, A metal-organic framework material that functions as an enantioselective catalyst for olefin epoxidation, Chem. Commun. 24 (2006) 2563–2565.
[14] L. Alaerts, E. Seguin, H. Poelman, F. Thibault-Starzyk, P.A. Jacobs, D.E. De Vos, Probing the Lewis acidity and catalytic activity of the metal-organic framework [Cu3(btc)2] (BTC = benzene-1,3,5-tricarboxylate), Chemistry 12 (2006) 7353–7363.
[15] M.H. Alkordi, Y. Liu, R.W. Larsen, J.F. Eubank, M. Eddaoudi, Zeolite-like metal-organic frameworks as platforms for applications: on metalloporphyrin-based catalysts, J. Am. Chem. Soc. 130 (2008) 12639–12641.
[16] F. Wilkinson, W.P. Helman, A.B. Ross, Quantum yields for the photosensitized formation of the lowest electronically excited singlet state of molecular oxygen in solution, J. Phys. Chem. Ref. Data 22 (1993) 113–262.
[17] M.F. Broglia, S.G. Bertolotti, C.M. Previtali, H.A. Montejano, Solvatochromic effects on the fluorescence and triplet–triplet absorption of phenosafranine in protic and aprotic solvents, J. Photochem. Photobiol. A 180 (2006) 143–149.
[18] M. González-Béjar, P. Montes-Navajas, H. Gracia, J.C. Scaiano, Methylene blue encapsulation in cucurbit[7]uril: laser flash photolysis and near-IR luminescence studies of the interaction with oxygen, Langmuir 25 (2009) 10490–10494.
[19] K.R. Gopidas, P.V. Kamat, Photophysics and photochemistry of phenosafranin dye in aqueous and acetonitrile solutions, J. Photochem. Photobiol. A. 48 (1989) 291–301.
[20] G. Calzaferri, N. Gfeller, Thionine in the cage of zeolite L, J. Phys. Chem. 96 (1992) 3428–3435.
[21] O. Varga, M. Kubinyi, T. Vidóczy, P. Baranyai, I. Bitter, M. Kállay, Methylene blue–calixarenesulfonate supramolecular complexes and aggregates in aqueous solutions, J. Photochem. Photobiol. A 207 (2009) 167–172.
[22] S. Easwaramoorthi, P. Natarajan, Spectral and electrochemical studies of methylene blue and thionine encapsulated in zeolite-Y, J. Porous Mater. 15 (2008) 343–349.
[23] M. Ehrl, H.W. Kindervater, F.W. Deeg, C. Braeuchle, R. Hoppe, Optical spectroscopy of thiazine and oxazine dyes in the cages of hydrated and dehydrated faujasite-type zeolites: molecular dynamics in a nanostructured environment, J. Phys. Chem. 98 (1994) 11756–11763.
[24] A.K. Shaw, S.K. Pal, Fluorescence relaxation dynamics of acridine orange in nanosized micellar systems and DNA, J. Phys. Chem. B 111 (2007) 4189–4199.
[25] B.S. Fujimoto, J.B. Clendenning, J.J. Delrow, P.J. Heath, M. Schurr, Fluorescence and photobleaching studies of methylene blue binding to DNA, J. Phys. Chem. 98 (1994) 6633–6643.
[26] S. Easwaramoorthi, P. Natarajan, Photophysical properties of phenosafranine (PHNS) adsorbed on the TiO_2-incorporated zeolite-Y, Microporous Mesoporous Mater. 86 (2005) 185–190.
[27] R. Schmidt, Influence of heavy atoms on the deactivation of singlet oxygen (1.DELTA.g) in solution, J. Am. Chem. Soc. 111 (1989) 6983–6987.
[28] B. Cojocaru, M. Laferrière, E. Carbonell, V. Parvulescu, H. García, J.C. Scaiano, Direct time-resolved detection of singlet oxygen in zeolite-based photocatalysts, Langmuir 24 (2008) 4478–4481.